Highly Active Porous Co-B Nanoalloy Synthesized on Liquid-Gas Interface for Hydrolysis of Sodium Borohydride

Xingpu Wang[a,c], Jinyun Liao[b], Hao Li[b], Hui Wang[c]*, Rongfang Wang[c], Bruno G. Pollet[d] and Shan Ji[a]*

[a] *College of Biological, Chemical Science and Chemical Engineering, Jiaxing University, Jiaxing, 314001, China*

[b] *School of Chemistry and Materials Engineering, Huizhou University, Huizhou 516007, China*

[c] *Institute of Chemical Engineering, Qingdao University of Science and Technology, Qingdao, 266042, China*

[d] *Department of Energy and Process Engineering, Faculty of Engineering, Norwegian University of Science and Technology (NTNU), NO-7491 Trondheim, Norway*

Corresponding authors:

Shan Ji (*): jisshan@126.com, Tel./fax: +86 (0)15024355548

Hui Wang (*): wanghui3931@126.com, Tel./fax: +86 (0)13919839172

Abstract:

Porous Co-B nanoalloy is a low-cost and highly active catalyst towards the hydrolysis of sodium borohydride ($NaBH_4$). In this study, a facile and room-temperature hydrogen bubble-assisted method was developed to prepare porous Co-B nanoalloy ($Co\text{-}B_{bubble}$) materials exhibiting high catalytic activity. The obtained materials are characterized by X-ray diffraction, scanning electron microscopy, energy-dispersive spectroscopy, X-ray photoelectron spectroscopy, inductively coupled plasma-optical emission spectrometer, transmission electron microscopy and surface area experiments. It is found that the hydrogen bubbles generated *in-situ* in the reaction system can act as template, which played an important role in determining the porous architecture of the final Co-B product. In the hydrolysis of sodium borohydride for hydrogen generation, the porous $Co\text{-}B_{bubble}$ nanoalloy materials exhibit high catalytic activity with mass normalized rate constant of 5.31 $L_{hydrogen}\ min^{-1}\ g_{catalyst}^{-1}$; a value which is much higher than those obtained for many other Co-B catalysts recently reported in the literature. The apparent activation energy (Ea) of the catalytic process is found to be ca. 30 kJ mol^{-1}. It is proposed that the high catalytic performance and low cost of $Co\text{-}B_{bubble}$ nanoalloy catalyst can be a promising material candidate in the hydrolysis of sodium borohydride for hydrogen production for commercial applications.

Keywords: Co-B alloy; Hydrogen bubble; Catalyst; Sodium borohydride; Hydrolysis

1. Introduction

The use of fossil fuels in the world causes drastic environmental pollution. The reduction in the consumption of fossil fuels and the development of "clean" energy is regarded as a feasible and possible way to minimize this serious global issue. In the last 20 years, extensive researches and efforts in renewable energy technologies have been one of the many pressing priorities for scientists and engineers [1]. As a type of renewable energy carrier, hydrogen is often seen as an "ideal" fuel due to its high energy density, its zero emission (when used in a fuel cell) and its abundant source [2-4]. There are many ways to produce H_2 from renewable resources. Generally, these H_2 production methods can be divided into two broad categories, namely biomass-based and water splitting technologies. Biomass technologies include thermochemical processes [5] and biological processes [6], and water splitting includes water electrolysis [7-10], thermolysis [11] and photo-electrolysis [12]. However, the utilization of hydrogen energy is severely restricted by how to safely and conveniently store hydrogen [13]. Compared to pressurized hydrogen [14] and cryogenic liquid hydrogen [15], reversible hydrogen storage materials such as metal/alloy hydrides [16-18], carbon materials [19], and complex hydrides [20-22] offer many benefits due to their high volumetric hydrogen capacities, acceptable energy efficiencies, and safety features. Recently, sodium borohydride ($NaBH_4$) has received great attention due to its high hydrogen capacity (with a theoretical value of 10.6 wt%), good storability, reaction controllability and low reaction initiating temperature [23]. Furthermore, the hydrolysis product, sodium metaborate ($NaBO_2$), is environmentally benign [24, 25]. Therefore, producing hydrogen by catalytic hydrolysis of sodium borohydride ($NaBH_4$) has attracted much research attention [23, 26]. For example, four (4) moles of hydrogen can be generated

by the hydrolysis of one (1) mole of sodium borohydride in the presence of an appropriate catalyst. Moreover, the catalytic hydrolysis of sodium borohydride in alkaline media is an attractive way to produce hydrogen due to its stability, high production rates and by-product reusability [27]. The reaction can be expressed as follows [28]:

$$NaBH_4 + 2H_2O \rightarrow 4H_2 + NaBO_2 + heat \quad (1)$$

To control and manage the self-hydrolysis of sodium borohydride, sodium hydroxide (NaOH), used as a stabilizer, is often added into the sodium borohydride solution [23]. The hydrolysis reaction is usually accelerated using various catalyst materials at ambient conditions [29]. Catalyst materials based on metals/alloys such as noble metals (Rh [30], Ru [31], Pd [32], Pt [33]) and transition metals (Ni [34], Ni-B [35], Co-W-B [36], Co-Ni-P-B [37] etc), have been extensively studied. The alloys of Co element and some semi-metal elements, such as Co-B and Co-P, have been shown to be effective and low-cost catalysts towards the hydrolysis of sodium borohydride. Practically, porous Co-B and Co-P catalyst materials are known to exhibit high activity in the dehydrogenation of sodium borohydride because they can provide numerous active sites for the hydrolytic reaction. In the literature, the synthesis of Co-B or Co-P alloys with porous structures using different fabrication methodologies is well-documented. For example, Tong *et al.* have synthesized porous honeycomb-like Co-B alloys by using triethanolamine as soft template [38]. Xu *et al.* prepared porous Co-P polyhedron materials with the use of a metal-organic framework as a hard template [39]. Very recently, Weng and co-workers described the fabrication of porous Co-P nanocatalysts by using Co-based zeolitic imidazolate framework as a template [40]. In these cases, either a hard template or a significant amount of capping agent is used in the synthesis,

which plays a crucial role in forming the porous structure of the final products. However, it was also found that the use of a capping agent or a hard template would increase the cost of the synthetic process. Moreover, the removal of these capping agents or hard templates from the surface of those nanocatalysts is very complicated and cumbersome. Therefore, it is of great significance to fabricate porous Co-B or Co-P nanoalloys without using any capping agents or hard templates.

In our previous work, we reported the preparation of PdNiP and PdCoP nanoalloys with net-like structures by a gas-liquid interface reaction, in which the externally introduced N_2 bubbles acted as a soft template [41, 42]. In this work, we modified this method, in which the hydrogen bubbles generated *in-situ* served as templates in the synthesis of porous Co-B nanoalloys. Compared with traditional template-based methods, our proposed method is more attractive due to the low cost of the templates i.e. the hydrogen bubbles. Moreover, it was observed that the removal of the templates was quite straight-forward as these hydrogen bubbles spontaneously burst. To the best of the authors´ knowledge, the synthesis of Co-B_{bubble} nanoalloy using hydrogen bubbles as soft templates has not been reported yet. It should be emphasized that no capping agents, such as surfactants, complexing agents or polymer stabilizers, are used in the synthesis. It is worth-mentioning that heterogeneous catalysis occurs at solid-gas or solid-liquid interfaces and the preparation of porous materials without the use of conventional templates can lead to no surface contamination [43]. Thus, the resultant Co-B material possesses a very "clean" surface, which is beneficial for catalytic reactions.

2. Experimental

2.1. Synthesis of porous Co-B_{bubble} nanoalloy catalysts

All reagents were of Analytic Grade (AR) and used as received. Double-distilled water was used in all experiments. Firstly, 100 mg $CoCl_2$•$6H_2O$ (99.0 %, Shanghai Zhongqin Chemical Reagent Co. Ltd) were dissolved in 50 mL H_2O to form a $CoCl_2$ solution and 100 mg $NaBH_4$ (96.0 %, Chinese Medicine Group Chemical Reagent Co. Ltd) were dissolved in another 50 mL H_2O to form a $NaBH_4$ solution. Secondly, a $CoCl_2$ solution was added dropwise into the $NaBH_4$ solution. The resultant Co-B was named as Co-$B_{no\ bubble}$. To prepare the Co-B_{bubble}, the collected powdery Co-$B_{no\ bubble}$ was mixed with a PTFE binder, which was then compacted on a Ni foam using an electric roller. The specification of the Ni foam, supplied by Suzhou Christie Bubble Pioneer Metals Corporation Co. Ltd, was as follows: the aperture was 0.2 nm, the porosity was 98 %, the through-hole rate was greater than 98 %, the surface density was 350 $g.m^2$, and the number of holes per inch was 110. The obtained Co-B/Ni film was then immersed in a 50 mL $NaBH_4$ solution (53 mM) and numerous hydrogen bubbles were generated. Subsequently, 50 mL $CoCl_2 \cdot 6H_2O$ solution (8.4 mM) were added dropwise into the $NaBH_4$ solution. A black precipitate was obtained and was named as Co-B_{bubble}. The above procedure is illustrated in Fig. 1.

Fig. 1 Synthetic procedure of Co-B_{bubble}

2.2. Characterizations

X-Ray diffraction (XRD) patterns were recorded using a PANalytical B. V. Empyean X-ray diffractometer with Cu-Kα radiation (λ = 1.5406 Å). The surface morphology and the elemental distribution of the nanoalloy catalysts were analysed using a Carl Zeiss Ultra Plus scanning electron microscope (SEM) equipped with an energy-dispersive spectroscopy (EDS). The specific surface area was determined by the Brunauer-Emmett-Teller (BET) method based upon the sorption isotherms obtained on a Quantachrome Autosorb-1 volumetric analyzer. The composition of the nanoalloys was determined by using a X-ray photoelectron spectroscopy (XPS) with a PHI-5702 multifunctional X-ray photoelectron spectrometer (Physical Electronics, San Francisco, CA, USA). Binding energies were determined by calibrating and referencing to the C 1*s* peak at 285.0 eV. Elementary analyses of the nanoalloy samples were performed using an inductively coupled plasma-optical emission spectrometer (ICP-OES) (Agilent 7700, Agilent Technologies Inc., Sydney, Australia). Transmission electron

microscopy (TEM) and selected area electron diffraction (SAED) patterns of the samples were obtained on a JEOL (JEM-2000 FX, JEOL Co., Kyoto, Japan) microscope operating at 200 kV.

2.3. Hydrogen generation measurement

The catalytic hydrolysis of $NaBH_4$ was carried out in a three-necked glass container connected to a gas burette to measure the accumulative volume of H_2 generated during the hydrolysis reaction. Typically, 2.7 mmol $NaBH_4$ and 2.5 mmol NaOH were mixed into the reaction vessel containing 10 ml of ultrapure water. For convenience, we defined the concentrations of 2.7 mmol $NaBH_4$ and 2.5 mmol NaOH as 1 wt%, followed by the addition of 10 mg Co-B catalyst under ultrasonication. The reaction temperature was set at 30 °C using a thermostated bath.

2.4. Kinetic studies

Kinetic data of the hydrolysis of $NaBH_4$ on fresh Co-B_{bubble} catalyst were generated by varying different process parameters such as: temperature, NaOH and $NaBH_4$ concentrations, and the amount of catalyst. For completeness, reusability of the catalyst was also explored. To obtain activation energy (E_a) values of the hydrolysis reaction catalyzed by Co-B_{bubble} and Co-$B_{no\ bubble}$ catalyst samples, the rates of H_2 generation were carefully measured at various temperatures, 25 °C, 30 °C, 35 °C and 40 °C. Other reaction parameters were also varied, for example, NaOH (0.25-2.0 mM) and $NaBH_4$ (0.25-4 mM) concentrations as well as the mass of the catalyst (2.5 mg-20 mg). Prior to studying reusability, the recovered powder was washed and dried using the same procedure as described above. This process was repeated 6 times in order to establish the reusability of the Co-B_{bubble} nanoalloy samples.

3. Results and Discussion

3.1. Catalyst characterization

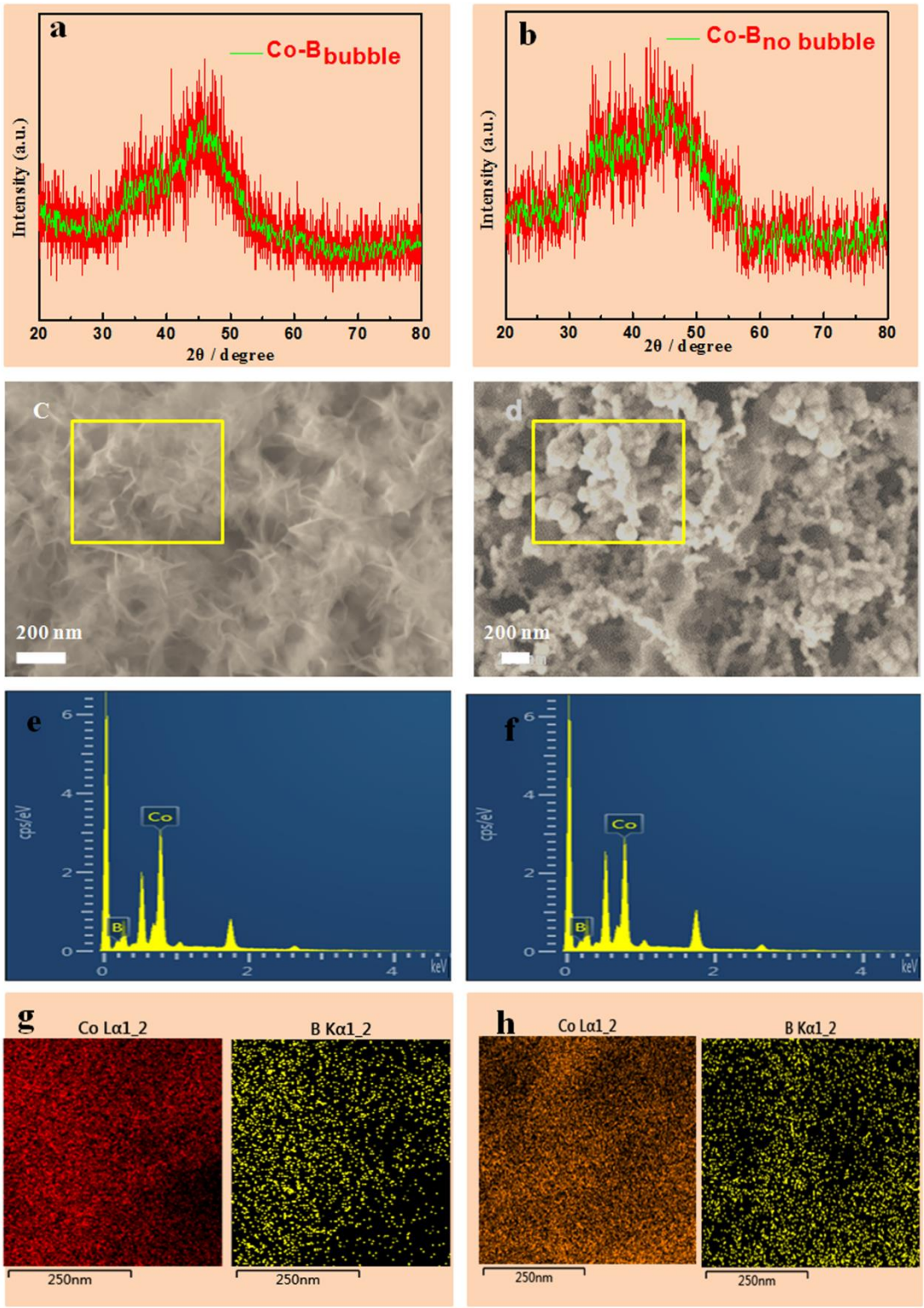

Fig. 2 XRD patterns of Co-B_{bubble} (a) and Co-$B_{no\ bubble}$ (b), SEM images of Co-B_{bubble} (c) and Co-$B_{no\ bubble}$ (d), the EDS spectra of the Co-B_{bubble} (e)and Co-$B_{no\ bubble}$ (f), the EDS mapping of Co and B elements for the Co-B_{bubble} (g)and Co-$B_{no\ bubble}$ (h).

Figs. 2(a-b) show the XRD patterns of the Co-B_{bubble} nanoalloy materials prepared in the absence and presence of hydrogen bubbles. Clearly, both samples show a weak wide peak at $2\theta \approx 45^{o}$, corresponding to the amorphous phase of Co-B alloy [44]. Figs. 2(c-d) display the SEM images of Co-B_{bubble} nanoalloys prepared in the absence and presence of hydrogen bubbles. As it can be observed from Fig. 2(c), the Co-B_{bubble} nanoalloy sample is composed of numerous sheet-like nanostructures. For comparison purposes, the morphology of the Co-$B_{no\ bubble}$ nanoalloy is shown in Fig. 2(d). It can also be observed that the produced Co-$B_{no\ bubble}$ nanoalloy is composed of nanoparticles with sizes ranging from 20 nm to 100 nm. Obviously, Co-B_{bubble} and Co-$B_{no\ bubble}$ have different geometric structures. However, the geometric structures determine the number of atoms located at the edges or corners, which can have a profound effect on the catalytic performance [45]. Figures 2(e) and 2(f) show the EDS spectra of Co-B_{bubble} and Co-$B_{no\ bubble}$ samples. As shown in Figs. 2(e) and 2(f), the peaks of Co are clear and strong, but the peaks of B are very small due to its low amount [46]. Figs. 2(g) and 2(h) show the EDX mapping of Co-B_{bubble} and Co-$B_{no\ bubble}$ catalyst samples, highlighting that the Co and B elements are evenly distributed in these samples, i.e. the Co and B elements are well mixed. The molar ratios of Co:B in the bulk Co-B_{bubble} and Co-$B_{no\ bubble}$ were determined to be ca. 1.82:1 and 4.18:1 respectively. Detailed information is shown in Table 1.

Table 1 Physical, chemical and catalytic properties of the catalysts

Sample	Composition (mol %)		S_{BET} (m^2/g)	Binding energy (eV)		HGR ($L_{hydrogen}\ min^{-1} g_{catalyst}^{-1}$)
	ICP results	XPS results		Co:2$p_{3/2}$	B:1s	
Co-B_{bubble}	$Co_{1.82}B$	$Co_{1.73}B$	82.1	778.2 and 783.3	189.1	5.31
Co-$B_{no\ bubble}$	$Co_{4.18}B$	$Co_{4.21}B$	26.2	778.3 and 783.4	189.2	2.48

a ICP results showing the bulk compositions of Co-B and the XPS results showing the surface compositions of Co-B.

b Binding energy data from XPS spectra.

c Hydrogen generation rates (HGR) were calculated based upon the active surface Co-B_{bubble} and Co-$B_{no\ bubble}$ metal for the hydrogen generation in 1 wt% NaOH solution, 1 wt% $NaBH_4$ solution and 10 mg catalyst at 40 °C.

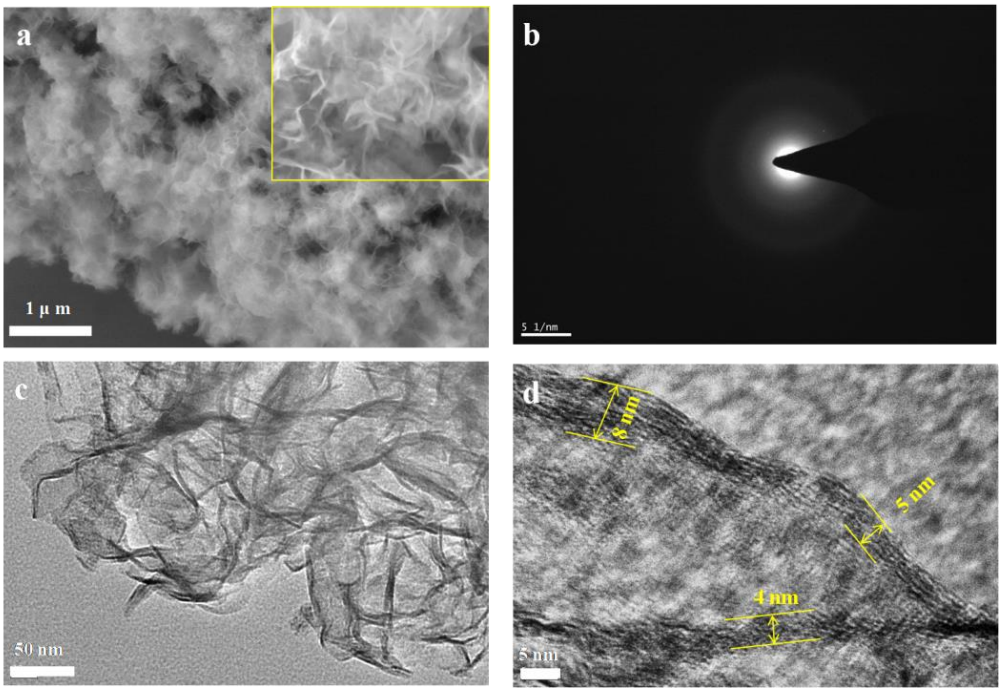

Fig. 3 SEM images (a), SAED pattern (b), TEM images (c) and (d) of the Co-B_{bubble} products. Inset in Fig. 3(a) shows the high magnification SEM image of catalyst

As it can be seen from Fig. 3(a), a low magnified SEM image, the Co-B_{bubble} nanoalloy possesses agglomerated particles. The inset of Fig. 3(a), a highly magnified

SEM image, shows that these agglomerated particles consisted of nanosheets. The SAED pattern of Co-B_{bubble} in Fig. 3(b) shows a continuous hollow ring corresponding to a diffraction pattern, typical of an amorphous structure [41, 42]. The microstructure was further investigated by TEM. As shown in Figs. 3(c) and 3(d), the Co-B_{bubble} nanoalloy is composed of numerous small nanosheets of several thicknesses of ca. 4 nm - 8 nm.

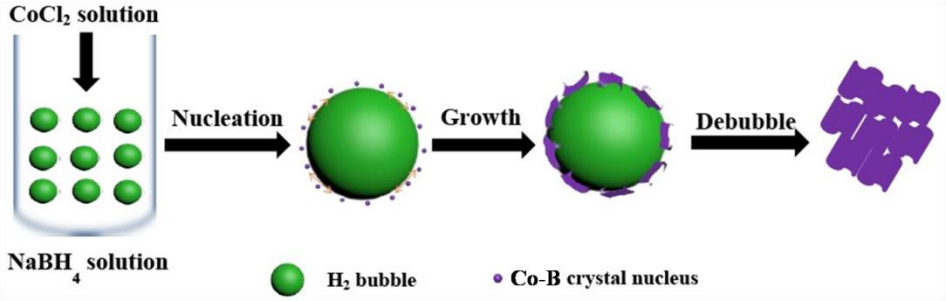

Fig. 4 Formation mechanism of Co-B_{bubble}.

In the reaction system, after the Co-$B_{no\ bubble}$/Ni foam was immersed in the $NaBH_4$ solution, numerous bubbles of hydrogen were generated via the catalytic hydrolytic reaction. When the $CoCl_2$ solution was added into the $NaBH_4$ solution, many Co-B nuclei were formed around the hydrogen bubbles. In this case, the hydrogen bubbles served as soft templates for the growth of Co-B nuclei. When the newly generated Co-B nanoclusters were added on the Co-B nuclei, they were allowed to grow along the external surface of the hydrogen bubbles. It was also observed that small curling nanosheets had been produced around the bubbles. After the bubbles burst, these small nanosheets gathered together to form a porous aggregate, as shown in Fig. 2(c). A possible formation mechanism is illustrated in Fig. 4. Once again, it should be noted that the hydrogen bubbles played a crucial role in determining the final morphology of the samples. In the absence of hydrogen bubbles as soft templates, only a few Co-B

nanoparticles were obtained, as shown in Fig. 2(d), since the self-hydrolysis of sodium borohydride at room temperature was sluggish [47].

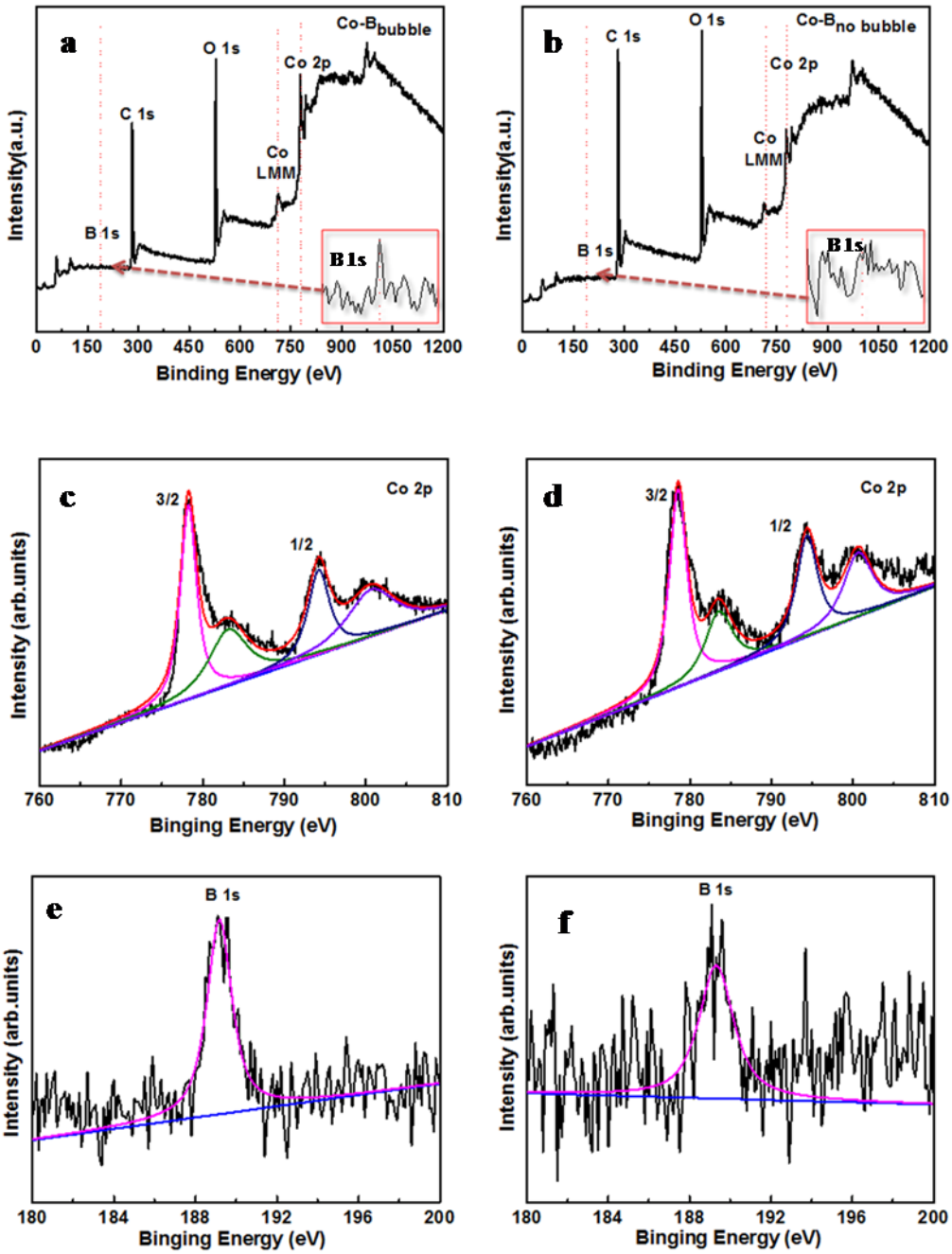

Fig. 5 X-ray photoelectron spectra of Co-B_{bubble} (a) and Co-$B_{no\ bubble}$ catalysts (b); Co 2*p* (c, d) and B 1*s* (e, f) of Co-B_{bubble} and Co-$B_{no\ bubble}$ samples respectively. Inset in Figs. 5(a) and 5(b) shows corresponding X-ray photoelectron spectra of B 1*s*.

Surface composition and elemental states of Co-B_{bubble} and Co-$B_{no\ bubble}$ were analyzed by XPS. Figs. 5(a) and 5(b) show the XPS spectra of the *as*-prepared Co-B_{bubble} and Co-$B_{no\ bubble}$ catalysts, highlighting that Co, B, O and C elements existed in the Co-B_{bubble} and Co-$B_{no\ bubble}$ samples. The relatively strong O element peak in the XPS spectra indicates that the surface of the catalysts was inevitably oxidized during sample preparation. Figs. 5(c) and 5(d) show high resolution XPS spectra of Co $2p_{3/2}$ of Co-B_{bubble} and Co-$B_{no\ bubble}$ samples respectively; and Figs. 5(e) and 5(f) show high resolution XPS spectra of B 1*s* of Co-B_{bubble} and Co-$B_{no\ bubble}$ catalysts respectively. The surface compositions and binding energies of each element in the samples are summarized in Table 1.

The XPS spectra of Co $2p_{3/2}$ in Co-B_{bubble} indicates the presence of cobalt species in metallic form and oxide state with binding energies (BE) of 778.2 and 783.3 eV respectively; values which are similar to those reported in the literature [48, 49]. The BE of Co $2p_{3/2}$ in Co-$B_{no\ bubble}$ is close to that of Co-B_{bubble}. For Co-B_{bubble}, the B 1*s* signal at 189.2 eV can be ascribed to elemental B in the amorphous borides, which is positively shifted by 2.1 eV compared to pure B (187.1 eV), indicating an electron transfer from alloying B to vacant *d*-orbital of metallic Co to make it rich electron and B deficient electron [50]. Moreover, the BE of B 1*s* in the Co-$B_{no\ bubble}$ sample is also close to Co-

B_{bubble} at 783.4 eV. It may be observed that the B content in the surface composition of the Co-B_{bubble} ($Co_{1.73}B$) nanoalloy is higher than that of the Co-$B_{no\ bubble}$ ($Co_{4.21}B$) based on the XPS spectra analyses. This finding may suggest that during reaction, the electron-enriched Co active sites "repels" the absorption of oxygen atoms while they are absorbed by the deficient electron B. In other words, the B element effectively keeps metal Co from oxidation [51]. In addition, for Co-B, the increased density of electron in Co could promote the hydrolysis of $NaBH_4$ [52]. Moreover, the electron-enriched metal active sites could facilitate the catalysis reaction by providing the electron to the hydrogen atom in hydridic form (H^-), which then might react with the water molecule to generate H_2 and OH^- ion. It has been previously shown that high electron density on active metal site is beneficial for promoting catalytic activity [53].

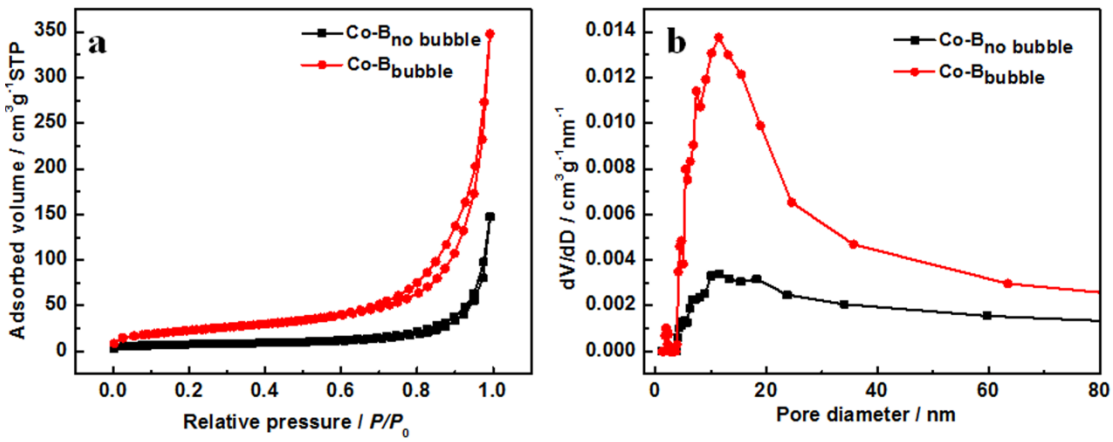

Fig. 6 N_2 adsorption-desorption isotherms (a) and the corresponding pore size distribution (b) of Co-B_{bubble} and Co-$B_{no\ bubble}$ samples

Fig. 6(a) displays the N_2 adsorption-desorption isotherms of the Co-B_{bubble} and Co-

$B_{no\ bubble}$. Both isotherms of the samples can be classified as *type II* isotherm in the classification of IUPAC [24]. A hysteresis loop in the range of the relative pressures from 0.6 to 0.97 is observed in the isotherm of Co-B_{bubble}, indicating the presence of mesopores. The corresponding pore size distribution curves using the Non-Local Density Functional Theory (NLDFT) method are presented in Fig. 6(b). The figure shows that the *as*-prepared mesoporous Co-B_{bubble} has a broad pore size distribution in the range of 3-35 nm. The Co-B_{bubble} sample exhibits a much higher N_2 sorption pore volume than that of Co-$B_{no\ bubble}$. The specific surface areas of Co-B_{bubble} and Co-$B_{no\ bubble}$ were calculated to be ca. 82.1 and 26.2 $m^2\ g^{-1}$ respectively. It was observed that the mesoporous channel is critical to improve diffusion and contact between catalyst and $NaBH_4$ [54, 55], and larger surface areas can provide more active sites for the hydrolysis of $NaBH_4$ [56]

3.2. Catalyst activity measurements

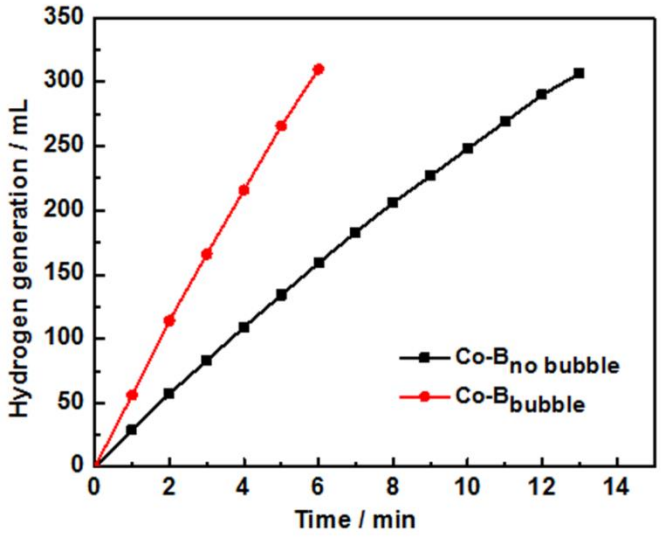

Fig. 7 Hydrogen generated in 1 wt% $NaBH_4$ and 1 wt% NaOH solution with 10 mg of Co-B_{bubble} or 10 mg of Co-$B_{no\ bubble}$ at 30 °C.

The catalytic behaviours of Co-$B_{no\ bubble}$ and Co-B_{bubble} samples were evaluated by the hydrolysis of $NaBH_4$ (as shown in Fig. 7) catalyzed on Ni foam. The experiments were performed under constant $NaBH_4$ and NaOH concentration (1 wt.%) at 30 °C and at a catalyst loading of 10 mg. It was found that no hydrogen was released from the $NaBH_4$ solution when Ni foam was used to catalyze this reaction, in other words, Ni foam was inactive toward the hydrolysis of $NaBH_4$. Various quantities of hydrogen was released from the $NaBH_4$ solution in the presence of Co-B_{bubble} and Co-$B_{no\ bubble}$ catalysts, hinting that both catalysts could catalyze the hydrolysis of $NaBH_4$. The hydrogen generation rate (HGR) of the catalytic hydrolytic process on the two samples can be calculated from the slope of the fitted lines in Fig. 7, which were found to be 24.8 mL min^{-1} for Co-$B_{no\ bubble}$ and 53.1 mL min^{-1} for Co-B_{bubble}, respectively. Taking the mass of the catalysts (10 mg) into account, the mass normalized rate constants were found to be 2.48 and 5.31 $L_{hydrogen}\ min^{-1}\ g_{catalyst}^{-1}$, respectively. It was also observed that Co-B_{bubble} exhibited significantly higher catalytic activity toward $NaBH_4$ hydrolysis than Co-$B_{no\ bubble}$. As previously discussed, the reason why Co-B_{bubble} show better catalytic performance than Co-$B_{no\ bubble}$ could be due to the fact that Co-B_{bubble} has larger BET surfaces, preferable mesoporous channel and enriched B surface composition. It was also found that the *as*-prepared Co-B_{bubble} catalyst exhibited a superior catalytic performance compared to other many Co-B catalysts reported in the literature, such as catkin-like Co-B catalysts [44], Co-B nanoparticles [57], unsupported Co-B catalysts [58], Co-B supported on carbon nanotubes [59], Co-B supported on Pd modified Ni foams [60] and TiO_2 doped Co-B catalysts [61]. However, the *as*-prepared catalysts exhibited lower catalytic activity than that of the recently reported Co-B supported on Ag-activated TiO_2 [23] and W-modified Co-B supported on Ag-activated

TiO_2 [62]. Detailed comparison of these catalysts are shown in Table 2.

Table 2 Comparison of HGR, durability and the activation energy between the *as*-prepared catalysts and other catalysts reported in the literature.

Catalyst used	HGR (L/min/g of catalyst)	Durability	Activation energy (kJ/mol)	Reference
Co	4.357	\[a]	56.53	[63]
Co	1.86	86.5 % after 10 cycles	38.194	[64]
Co	1.596	57.72% after5 cycles	37.01	[65]
Co	2.864	72% after 5 cycles	43.26	[66]
Co-B	3.12	88% after 8 cycles	\[a]	[44]
Co-B	4.38	\[a]	\[a]	[38]
Co-B	3.35	\[a]	40	[67]
Co-B	2.16	\[a]	45.5	[68]
Co-B	4.62	\[a]	no	[69]
Co-B	4.928	\[a]	42.3	[70]
Co-B	5	\[a]	30	[71]
Co-B	2.4	\[a]	\[a]	[58]
Co-B	2.97	\[a]	\[a]	[34]
Co-P-B	4.0	\[a]	32	[53]
Co-Fe-B	1.3	\[a]	31	[72]
Co-B/clay	1.270	68.6 % after 9 cycles	56.32	[73]
Co-B/C	5.1	\[a]	40.4	[59]
Co-B/Pd- Ni foam	2.875	\[a]	\[a]	[60]
Co-B/TiO2	1.98	\[a]	30,93	[61]
Co-W-P	5	49 % after 5 cycles	22.8	[74]
Co-B/Ni foam	1.640	\[a]	44.47	[75]
Co-B/Ag- Ni foam	6.294	70 % after 5 cycles	44	[23]
W-Co-B/Ag-Ni foam	7.27	50 % after 5 cycles	\[a]	[62]

Co-B	5.31	79.3 % after 5 cycles	30	This study

[a] Not reported or no detailed data are available

3.3. Kinetic studies

3.3.1. Effect of NaOH concentration

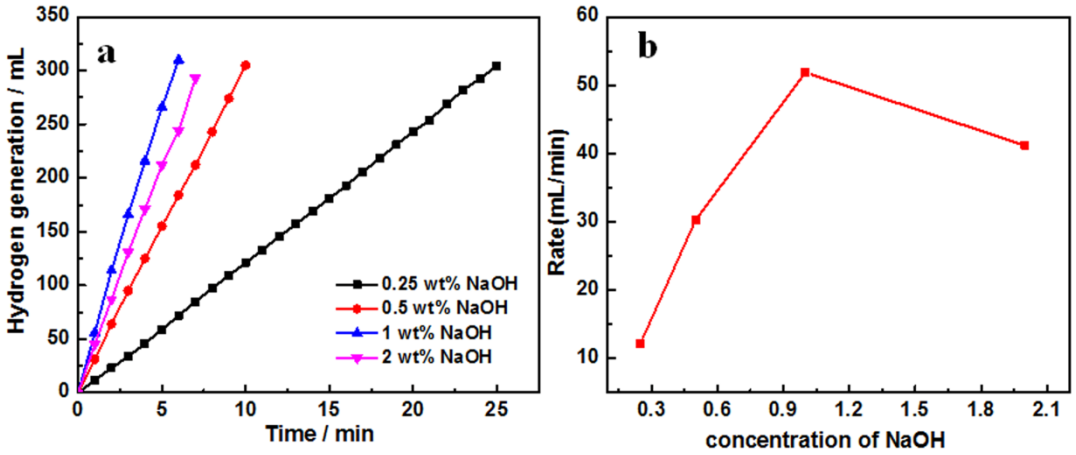

Fig. 8 Effect of NaOH concentration on hydrogen generation: 10 mg Co-B_{bubble} and $NaBH_4$ (1 wt%) at 30 °C (a); relationship between NaOH concentration and hydrogen generation (b).

NaOH concentrations were varied from 0.25 wt% to 2 wt% to investigate the effect of NaOH concentration on the hydrolysis of $NaBH_4$. During the experiments, the concentration of $NaBH_4$ was maintained at 1 wt%, the catalyst loading was fixed at 10 mg and the temperature was kept at 30 °C. Fig. 8(a) shows a plot of volume of hydrogen *vs* time at different NaOH concentrations. The figure shows that the HGR increases with increased NaOH concentration. When the NaOH concentration continuously increased to 2 wt. %, it was observed that the HGR was lower than the HGR at 1 wt. % NaOH solution. This finding indicates that NaOH concentration affects $NaBH_4$

hydrolysis. Moreover, the hydrolysis reaction can be impeded when there are too much OH^- ions in the solution, possibly in turns decreasing $NaBO_2$ solubility and allowing insoluble material to be deposited on the surface of catalyst and thus blocking active sites [76]. As shown in Fig. 8(b), the plot HGR *vs.* NaOH concentration exhibits a volcano-like curve. It can be observed from the figure that when the concentration of NaOH was 1 wt. %, the HGR reached a maximum value of ca. 55 mL/min.

3.3.2. Effect of catalyst concentration

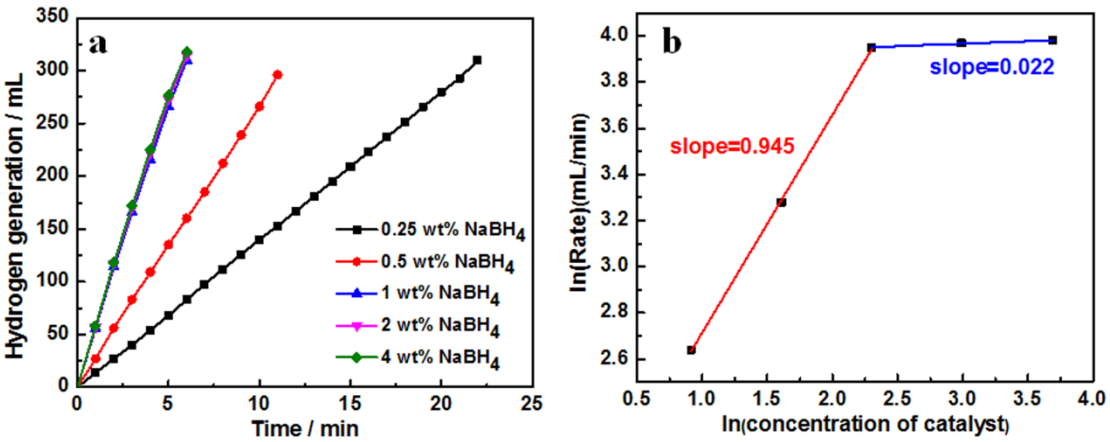

Fig. 9 (a) Effect of catalyst loading on hydrogen generation and (b) plot of ln(hydrogen generation rate) versus ln(catalyst loading) (b).

To investigate the effect of catalyst loading on the hydrogen generation, $NaBH_4$ hydrolysis experiments were carried out at various catalyst loadings in $NaBH_4$ (1 wt. %) and NaOH (1 wt. %) solutions and at 30 °C, as shown in Fig. 9. As expected, the HGR increases with catalyst loadings. The figure also shows that the plot of ln(HGR) *vs.* ln(catalyst concentration) yields a straight line. The slope of this straight line provides

the value of order of reaction with respect to catalyst concentration. The value of the slope was found to be 0.94, indicating that the hydrolysis of $NaBH_4$ is a first order reaction on Co-B_{bubble} catalyst.

3.3.3. Effect of temperature

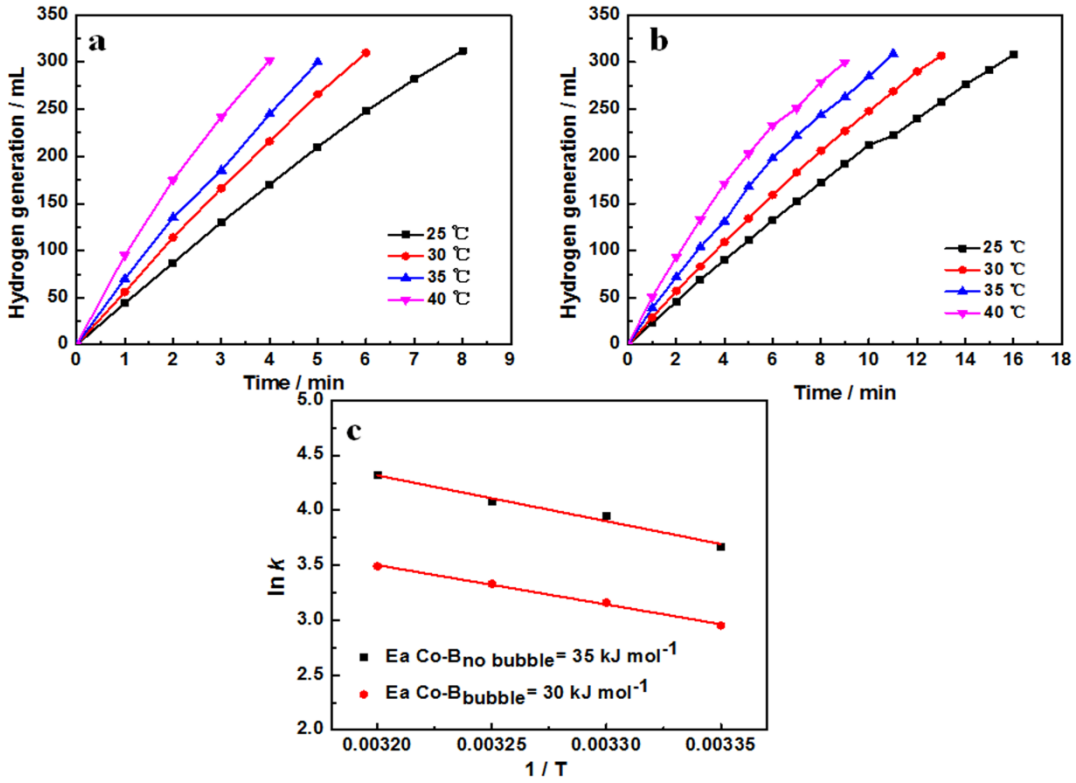

Fig. 10 Effect of temperature on hydrogen generation ($NaBH_4$: 1 wt.%, NaOH: 1 wt.% and catalyst loading: 10 mg) on Co-B_{bubble} (a) and of Co-$B_{no\ bubble}$ (b), *Arrhenius* plots of $NaBH_4$ hydrolysis rates on Co-B_{bubble} and Co-$B_{no\ bubble}$ (c).

It is well-known that the reaction temperature affects the rate constants of the catalytic hydrolysis of $NaBH_4$. In this study, the $NaBH_4$ hydrolysis was carried out in the temperature range [25 °C - 40 °C]. Figs. 10(a) and 10(b) depict the relationship between the rates of hydrogen generation and the hydrolysis temperatures in the

presence of Co-B_{bubble} and Co-$B_{no\ bubble}$ as catalysts, respectively. For both catalysts, it can be observed that increasing the reaction temperature can improve the reaction rate of $NaBH_4$ hydrolysis. For example, when the Co-B_{bubble} acted as a catalyst, it took ca. 7.6 min to generate 300 mL hydrogen at a reaction temperature of 30 °C. In contrast, it took only about 4 min to produce 300 mL hydrogen at 40 °C. According to the *Arrhenius* equation:

$$\ln k = -\frac{E_a}{RT} + \ln A \qquad (2)$$

where k is the rate constant of the reaction; E_a represents the activation energy of the reaction (kJ mol^{-1}); A is pre-exponential factor; R is molar gas constant (8.314 J K^{-1} mol^{-1}); T is thermodynamic temperature of the reaction (K). The apparent activity energy (E_a) can be calculated based upon the data of the reaction rates obtained at different temperatures.

The apparent activity energy values were found to be 35 kJ mol^{-1} for the Co-$B_{no\ bubble}$ catalyst, and 30 kJ mol^{-1} for the Co-B_{bubble} catalyst (Fig. 10(c)). The relatively low E_a of Co-B_{bubble} catalyst further demonstrates that it exhibits higher catalytic activity than Co-$B_{no\ bubble}$ catalysts. The comparison of the E_a values of the *as*-prepared catalysts with other catalysts reported in the literature can also be found in Table 2.

3.3.4. Effect of $NaBH_4$ concentration

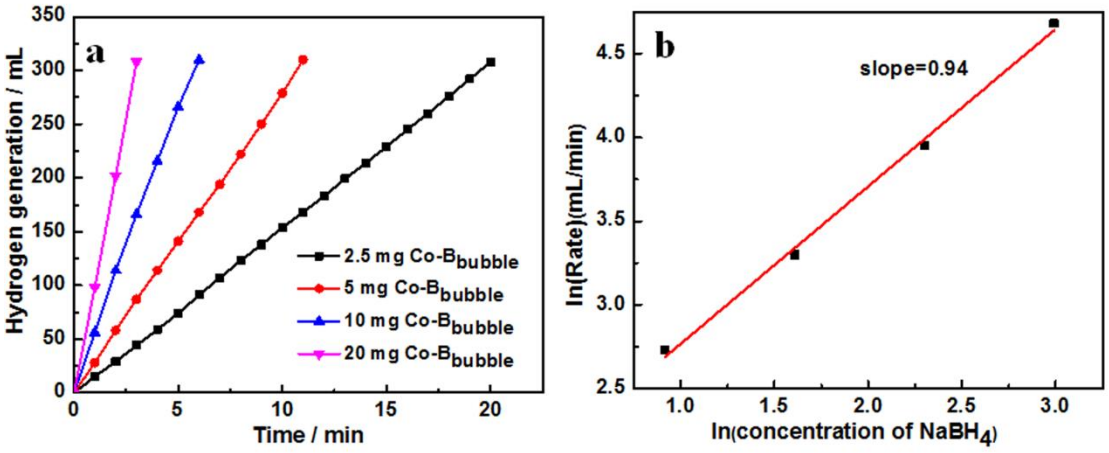

Fig. 11 (a) Effect of $NaBH_4$ concentration on hydrogen generation and (b) plot of hydrogen generation rate versus $NaBH_4$ concentration (both in natural logarithmic scale).

In terms of the reaction order of $NaBH_4$ hydrolysis under various $NaBH_4$ concentrations, there are several conflicting findings in the literature. A few researchers reported a zero-order kinetics for $NaBH_4$ hydrolysis [77, 78]. First order kinetics was also observed by other workers [79, 80].

In order to shed some light and gain a better understanding of $NaBH_4$ hydrolysis, a wide range of $NaBH_4$ molar concentrations (0.25 wt%, 0.5 wt%, 1 wt%, 2 wt%, 4 wt%) were used on the *as*-prepared catalysts. As shown in Figure 11(a), the HGR increases with $NaBH_4$ concentrations in the range of 0.25 wt% to 1 wt%. When the $NaBH_4$ concentration is higher than 1 wt. %, it can be observed that the HGR does not significantly change with concentration. A linear plot of ln(HGR) *vs* ln($NaBH_4$ concentration) is shown in Fig. 11(b), with a slope of 0.945, indicating that the $NaBH_4$ hydrolysis is a first order reaction when $NaBH_4$ concentration is lower than 1 wt. %. When the $NaBH_4$ concentration is higher than 1 wt.%), $NaBH_4$ hydrolysis exhibits a zero-order kinetics with respect to $NaBH_4$ concentration.

The above findings clearly show that the order of reaction depends upon $NaBH_4$ concentrations. It varies from 1 to 0 as the concentration is increased. To gain a better insight, two simple processes were carried out to study the catalytic hydrolysis reaction of $NaBH_4$ on the surface of the nanoalloy catalysts [81, 82]: (i) catalytic absorption of BH_4^- on the surface of the active sites, and (ii) reaction of the absorbed species to generate H_2. When the $NaBH_4$ concentration is low, the hydride/catalyst molar ratio is also low indicating that the surface of the catalyst is not fully occupied by the BH_4^- reactants, and there are some active sites available on the surface. Thus, the first order kinetics involving the diffusion of BH_4^- on the catalyst surface is the rate limiting step. At high hydride/catalyst molar ratio, a zero-order kinetics is predominant because the reaction mechanism shows opposite results in the case of low hydride/catalyst molar ratio.

For any chemical reactions, the reaction rate (r) is given by the power law [83] which is written as:

$$r = A \exp(-Ea/RT)\ [\text{reactants}]^a \qquad (3)$$

where A is a pre-exponential factor; Ea is the activation energy; R is the universal gas constant; T is the temperature and, a is the order of reaction.

During the catalytic hydrolysis of $NaBH_4$ in alkaline solutions, the hydrogen generation rate depends upon many factors, such as temperature, the catalyst loading, $NaBH_4$ and NaOH concentrations. Thus, Equation (2) can be written as:

$$r = A \exp(-Ea/RT)\ [\text{catalyst}]^x\ [NaBH_4]^y \qquad (3)$$

where x and y are the reaction orders with respect to catalyst loading and $NaBH_4$ concentration respectively.

Thus, the reaction rate on Co-B_{bubble} catalyst can be determined according to the

above findings.

At low NaBH4 concentrations, the kinetics can be described as first-order:

$r = A \exp(-Ea/RT)\ [\text{catalyst}]^{0.94}\ [NaBH_4]^{0.945} \approx A \exp(-Ea/RT)\ [\text{catalyst}]\ [NaBH_4]$

At high $NaBH_4$ concentrations, the kinetics can be described as zero-order:

$r = A \exp(-Ea/RT)\ [\text{catalyst}]^{0.94}\ [NaBH_4]^{0.022} \approx A \exp(-Ea/RT)\ [\text{catalyst}]$

3.3.5. Reusability and stability of Co-B_{bubble}

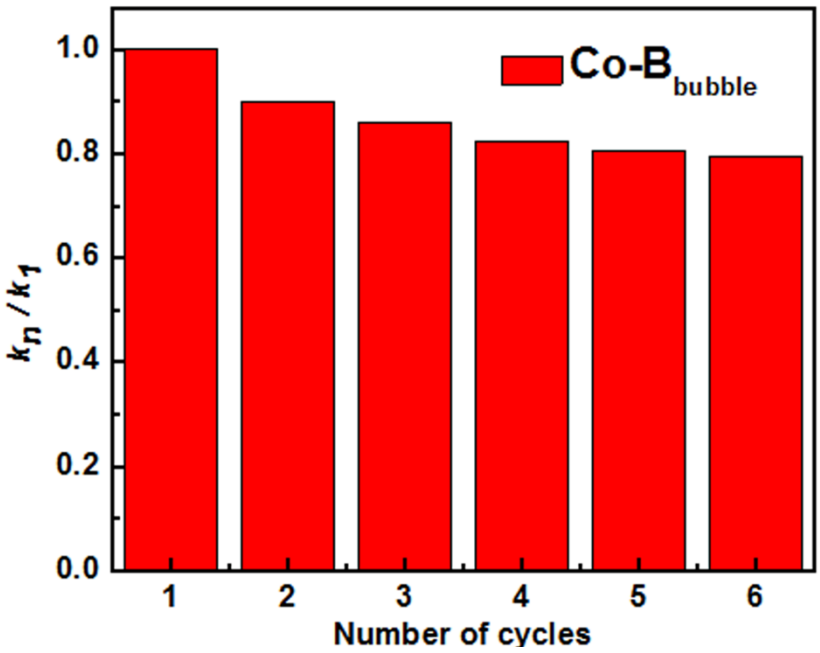

Fig. 12 Reusability experiments for the Co-B_{bubble} catalyst

Catalyst reusability is very vital for its practical application in industrial hydrogen generation. Fig. 12 shows the rate constant of $NaBH_4$ hydrolysis at various catalytic cycle numbers. As it can be seen from the figure, the rate constants of the catalytic hydrolysis of $NaBH_4$ gradually decrease as the cycle number increases. When the cycle number reaches 6, its activity remains at 79.3 % of its initial activity, indicating that the Co-B_{bubble} possesses relatively good reusability. A detailed comparison of the *as*-prepared catalyst reusability with other Co-based catalysts reported in literature is presented in Table 2.

4. Conclusions

A facile, low-cost and environmentally-friendly hydrogen bubble-assisted synthesis of porous Co-B_{bubble} nanoalloy at room temperature was described. It was found that the hydrogen bubble generated *in-situ* from the Co-$B_{no\ bubble}$/Ni foam catalysts, the $NaBH_4$ solution in the reaction system can act as a soft template, which plays a crucial role in determining the porous architecture of the Co-B product. In the hydrolysis of sodium borohydride for hydrogen generation, the porous Co-B_{bubble} nanoalloy exhibited high catalytic activity and the apparent activation energy of the catalytic process was determined to be ca. 30 kJ mol^{-1}. It was also found that the high catalytic performance and low cost of the porous Co-B_{bubble} nanoalloy material could be a promising catalyst candidate in the hydrolysis of sodium borohydride for hydrogen production for commercial applications. Moreover, the hydrogen bubble-based template synthesis could be extended to the preparation of other alloy catalysts, such as Co-P, Ni-B and Co-Ni-B.

Acknowledgements

This work is financially supported by the Natural Science Foundation of China (No. 51661008 and No.51362027), the Natural Science Foundation of Guangdong Province (No. 2016A030313120), the Excellent Youth Foundation of the University in Guangdong Province (No. YQ2015154) and Natural Science Foundation of Huizhou University (No. 20160226013501332).

References:

[1] Lund H, Mathiesen B. Energy system analysis of 100 % renewable energy systems—The case of Denmark in years 2030 and 2050. Energy. 2009;34:524-5314.
[2] Barbir F. Transition to renewable energy systems with hydrogen as an energy carrier.

Energy. 2009;34:308-12.
[3] Marino C, Nucara A, Pietrafesa M, Pudano A. An energy self-sufficient public building using integrated renewable sources and hydrogen storage. Energy. 2013;57:95-105.
[4] Li H, Liao J, Zhang X, Liao W, Wen L, Yang J, et al. Controlled synthesis of nanostructured Co film catalysts with high performance for hydrogen generation from sodium borohydride solution. Journal of Power Sources. 2013;239:277-83.
[5]Liu S, Zhu J, Chen M, Xin W, Yang Z, Kong L. Hydrogen production via catalytic pyrolysis of biomass in a two-stage fixed bed reactor system. International Journal of Hydrogen Energy. 2014;39:13128–35.
[6]Das D. Hydrogen production by biological processes: a survey of literature. International Journal of Hydrogen Energy. 2001;26:13–28.
[7] Jing S, Lu J, Yu G, Yin S, Luo L, Zhang Z, et al. Advanced Materials. 2018, 1705979-86.
[8] Jing S, Zhang L, Luo L, Lu J, Yin S, Shen P, et al. N-Doped porous molybdenum carbide nanobelts as efficient catalysts for hydrogen evolution reaction. Applied Catalysis B: Environmental. 2018;224:533–40.
[9] Lu J, Zhang L, Jing S, Luo L, Yin S. Remarkably efficient PtRh alloyed with nanoscale WC for hydrogen evolution in alkaline solution. International Journal of Hydrogen Energy. 2017;42:5993-9.
[10] Zhang L, Lu J, Yin S, Luo L, Jing S, Brouzgoue A, et al. One-pot synthesized boron-doped RhFe alloy with enhanced catalytic performance for hydrogen evolution reaction. Applied Catalysis B: Environmental. 2018;230:58–64.
[11] Flamos a, Georgallis P, Doukas H, Psarras J. Using biomass to achieve European Union energy targets—a review of biomass status, potential, and supporting policies. International Journal of Green Energy. 2011;8:411–28.
[12] Kothari R, Buddhi D, Sawhney R. Comparison of environmental and economic aspects of various hydrogen production methods. Renewable Sustainable Energy Reviews. 2008;12:553–63.
[13] Ziogou C, Ipsakis D, Seferlis P, Bezergianni S, Papadopoulou S, Voutetakis S. Optimal production of renewable hydrogen based on an efficient energy management strategy. Energy. 2013;55:58-6.
[14] Aceves S, Martinez-Frias J, Garcia-Villazana O, Analytical and experimental evaluation of insulated pressure vessels for cryogenic hydrogen storage. International Journal of Hydrogen Energy. 2000;25:1075–85.
[15] Dillon A, Jones K, Bekkedahl T, Kiang C, Bethune D, Heben M. Storage of hydrogen In singal-walled carbon nanotubees. Nature. 1997;386:377–9.

[16] Ismail M. Effect of $LaCl_3$ addition on the hydrogen storage properties of MgH_2. Energy. 2015;79:177-82.
[17] Fan M, Liu S, Zhang Y, Zhang J, Sun L, Xu F. Superior hydrogen storage properties of MgH_2-10 wt% TiC. Energy. 2010;35:3417-21.
[18] Biniwale R, Rayalu S, Devotta S, Ichikawa M. Chemical hydrides: a solution to high capacity hydrogen storage and supply. International Journal of Hydrogen Energy. 2008;33:360-5.
[19] Gross K, Thomas G, Jensen C. Catalyzed alanates for hydrogen storage. Journal of Alloys Componds. 2002;330-332:683-90.
[20] Zuttel A, Wenger P, Rensch S, Sudan P, Mauron P, Emmenegger C. $LiBH_4$ a new hydrogen storage material. Journal of Power Sources. 2003;118:1-7.
[21] Eberle U, Felderhoff M, Schuth F. Chemical and physical solutions for hydrogen storage. Angewandte chemie international edition. 2009;48:6608-30.
[22] Bakker S. Hydrogen patent portfolios in the automotive industry e the search for promising storage methods. International Journal of Hydrogen Energy. 2010;35:6784-93.
[23] Shen X, Wang Q, Wu Q, Guo S, Zhang Z, Sun Z, et al. CoB supported on Ag-activated TiO_2 as a highly active catalyst for hydrolysis of alkaline $NaBH_4$ solution. Energy. 2015;90:464-74.
[24] Turhan T, Güvenilir Y, Sahiner N. Micro poly(3-sulfopropyl methacrylate) hydrogel synthesis for in situ metal nanoparticle preparation and hydrogen generation from hydrolysis of $NaBH_4$. Energy. 2013;55:511-8.
[25] Chinnappan A, Jadhav A, Puguan J, Appiah-Ntiamoah R, Kim H. Fabrication of ionic liquid/polymer nanoscale networks by electrospinning and chemical cross-linking and their application in hydrogen generation from the hydrolysis of $NaBH_4$. Energy. 2015;79:482-8.
[26] Xi L, Su J, Wang K, Du G, Asin A, Sun X. Properties of CuCoP/γ-AI_2O_3 catalysts for efficient hydrogen generation by hydrolysis of alkaline $NaBH_4$ solution. International Journal of Hydrogen Energy. 2017;42:30639-45.
[27] Kong V, Kirk D, Foulkes F, Hinatsu J. Development of hydrogen storage for fuel cell generators II: utilization of calcium hydride and lithium hydride. International Journal of Hydrogen Energy. 2003;28:205-14.
[28] Şahin Ö, Kilinç D, Saka C. Hydrogen production by catalytic hydrolysis of sodium borohydride with a bimetallic solid-State Co-Fe complex catalyst. Separation Science & Technology. 2015;50:2015-2019.
[29] Kojima Y, Suzuki K, Fukumoto K, Kawai Y, Kimbara M, Nakanishi H, et al. Development of 10 kW-scale hydrogen generator using chemical hydride. Journal of

Power Sources. 2004;125:22-6.
[30] Larichev Y, Netskina O, Komova O, Simagina V. Comparative XPS study of Rh/Al_2O_3 and Rh/TiO_2 as catalysts for $NaBH_4$ hydrolysis. International Journal of Hydrogen Energy. 2010;35:6501-7.
[31] Keçeli E, Özkar S. Ruthenium(III) acetylacetonate: A homogeneous catalyst in the hydrolysis of sodium borohydride. Journal of Molecular Catalysis A Chemical. 2008;286:87-91.
[32] Patel N, Patton B, Zanchetta C, Fernandes R, Guella G, Kale A, et al. Pd-C powder and thin film catalysts for hydrogen production by hydrolysis of sodium borohydride. International Journal of Hydrogen Energy. 2008;33:287-92.
[33] Xu D, Zhang H, Ye W. Hydrogen generation from hydrolysis of alkaline sodium borohydride solution using Pt/C catalyst. Catalysis Communications. 2007;8:1767-71.
[34] Şahin Ö, Saka C, Baytar O, Hansu F. Influence of plasma treatment on electrochemical activity of Ni(0)-based catalyst for hydrogen production by hydrolysis of $NaBH_4$. Journal of Power Sources. 2013;240:729-35.
[35] Lee J, Ann H, Yi Y, Lee K, Uhm S, Lee J. A stable Ni–B catalyst in hydrogen generation via $NaBH_4$ hydrolysis. Catalysis Communications. 2011;16:120-3.
[36] Ekinci A, Şahin Ö, Saka C, Avci T. The effects of plasma treatment on electrochemical activity of Co–W–B catalyst for hydrogen production by hydrolysis of $NaBH_4$. International Journal of Hydrogen Energy. 2013;38:15295-301.
[37] Fernandes R, Patel N, Miotello A. Efficient catalytic properties of Co–Ni–P–B catalyst powders for hydrogen generation by hydrolysis of alkaline solution of $NaBH_4$. International Journal of Hydrogen Energy. 2009;34:2893-900.
[38] Tong D, Chu W, Wu P, Zhang L. Honeycomb-like Co–B amorphous alloy catalysts assembled by a solution plasma process show enhanced catalytic hydrolysis activity for hydrogen generation. Rsc Advances. 2012;2:2369-76.
[39] Xu M, Han L, Han Y, Yu Y, Zhai J, Dong S. Porous CoP concave polyhedron electrocatalysts synthesized from metal–organic frameworks with enhanced electrochemical properties for hydrogen evolution. Journal of Materials Chemistry A. 2015;3:21471-7.
[40] Weng B, Wei W, Wu H, Alenizi A, Zheng G. Bifunctional CoP and CoN porous nanocatalysts derived from ZIF-67 in situ grown on nanowire photoelectrodes for efficient photoelectrochemical water splitting and CO_2 reduction. Journal of Materials Chemistry A. 2016;4.
[41] Wang R, Ma Y, Wang H, Key J, Ji S. Gas-liquid interface-mediated room-temperature synthesis of "clean" PdNiP alloy nanoparticle networks with high catalytic activity for ethanol oxidation. Chemical Communications. 2014;50:12877.

[42] Ma Y, Wang R, Wang H, Key J, Ji S. Room-temperature synthesis with inert bubble templates to produce "clean" PdCoP alloy nanoparticle networks for enhanced hydrazine electro-oxidation. Rsc Advances. 2015;5:9837-42.
[43] Tao F, Peter A. Crozier Atomic-Scale Observations of Catalyst Structures under Reaction Conditions and during Catalysis. Chemical Reviews. 2016, 116, 3487-3539.
[44] Yan J, Liao J, Li H, Feng K, Wang H, Wang R, et al. Capping-agent-free Synthesis of Catkin-like CoB Microstrucutres Composed of Untrathin Nanosheets and Their Catalytic Performance in the Hydrolysis of Sodium Borohydride. International Jounal of Electrochemical Science. 2016;11:226-32.
[45] Bond G, Small particles of the Platinum metals. Platinum Metals Review. 1975;19:126-34.
[46] Wang S. Electroless deposition of Ni–Co–B alloy films and influence of heat treatment on the structure and the magnetic performances of the film. Thin Solid Films. 2007;515:8419–23.
[47] Kreevoy M, Jacobson R. The rate of decomposition of $NaBH_4$ in basic aqueous solutions. Ventron Alembic. 1979;15:2-3.
[48] Li H, Chen X, Wang M, Xu Y. Selective hydrogenation of cinnamaldehyde to cinnamylalcohol over an ultrafine Co-B amorphous alloy catalyst. Applied Catalysis. A: General. 2005;225:117-30.
[49] Christoskovaa S, Stoyanovaa M, Georgievaa M, Mehandjiev D. Materials chemistry and physics. 1999;60:39-43.
[50] Patel N, Guella G , Kale A, Miotello A , Patton B , Zanchetta C, et al. Thin films of Co–B prepared by pulsed laser deposition as efficient catalysts in hydrogen producing reactions. Applied Catalysis A: General 2007;323:18–24.
[51] Patel N, Miotello A. Progress in Co-B related catalyst for hydrogen production by hydrolysis of boron-hydrides: review and the perspectives to substitute noblemetals. International Journal of Hydrogen Energy. 2015;40:1429-64.
[52] Guella G, Zanchetta C, Patton B, Miotello A. New insights on the mechanism of palladium-catalyzed hydrolysis of sodium borohydride from ^{11}B NMR measurements. The Journal of Physical Chemistry B. 2006;110:17024-33.
[53] Patel N, Fernandes R, Miotello A. Hydrogen generation by hydrolysis of $NaBH_4$ with efficient Co–P–B catalyst: A kinetic study. Journal of Power Sources. 2009;188: 411–20.
[54] Tong D, Han X, Chu W, Chen H, Ji X. Preparation of, mesoporous Co-B catalyst via self-assembled triblock copolymer templates. Materials Letters. 2007;61:4679-82.
[55] Tong D, Zeng X, Chu W, Wang D, Wu P. Magnetically recyclable hollow Co-B nanospindles as catalysts for hydrogen generation from ammonia borane. Journal of

Materials Science. 2010;45:2862-7.
[56] Loghmani M, Shojaei A. Hydrogen generation from hydrolysis of sodium borohydride by cubic Co-La-Zr-B nano particles as novel catalyst. International Journal of Hydrogen Energy. 2013;38:10470-8.
[57] Brunauer S, Deming L, Deming W, Teller E. On a Theory of the van der Waals Adsorption of Gases. Journal of the American Chemical Society. 1940;62:1723-32.
[58] Jeong S, Cho E, Nam S, Oh I, Jung U, Kim S. Effect of preparation method on Co–B catalytic activity for hydrogen generation from alkali $NaBH_4$ solution. International Journal of Hydrogen Energy. 2007;32:1749-54.
[59] Huang Y, Yi W, Zhao R, Pei K, Wei Z. Accurately measuring the hydrogen generation rate for hydrolysis of sodium borohydride on multiwalled carbon nanotubes/Co–B catalysts. International Journal of Hydrogen Energy. 2008;33:7110-5.
[60] Lee J, Kong K, Chang R, Cho E, Yoon S, Han J, et al. A structured Co–B catalyst for hydrogen extraction from $NaBH_4$ solution. Catalysis Today. 2007;120:305-10.
[61] Cheng J, Xiang C, Zou Y, Chu H, Qiu S, Zhang H, et al. Highly active nanoporous Co–B–TiO_2 framework for hydrolysis of $NaBH_4$. Ceramics International. 2015;41:899-905.
[62] Shen X, Wang Q, Guo S, Liu B, Sun Z, Zhang Z, et al. W-modified CoB supported on Ag-activated TiO_2 for hydrogen generation from alkaline NaBH 4 solution. International Journal of Hydrogen Energy. 2015;40:6346-57.
[63] Sahiner N, Yasar A, Aktas N. Dicationic poly(4-vinyl pyridinium) ionic liquid capsules as template for Co nanoparticle preparation and H_2 production from hydrolysis of $NaBH_4$. Angewandte chemie international edition. 2015;23:100-8.
[64] Seven F, Sahiner N. Metal ion-imprinted hydrogel with magnetic properties and enhanced catalytic performances in hydrolysis of $NaBH_4$ and NH_3BH_3. International Journal of Hydrogen Energy. 2013;38:15275-84.
[65] Seven F, Sahiner N. Superporous P(2-hydroxyethyl methacrylate) cryogel-M (M: Co, Ni, Cu) composites as highly effective catalysts in H_2 generation from hydrolysis of $NaBH_4$ and NH_3BH_3. International Journal of Hydrogen Energy. 2014;39:15455-63.
[66] Turhan T, Güvenilir Y, Sahiner N. Micro poly(3-sulfopropyl methacrylate) hydrogel synthesis for in situ metal nanoparticle preparation and hydrogen generation from hydrolysis of $NaBH_4$. Energy. 2013;55:511-8.
[67] Gupta S, Patel N, Fernandes R, Kothari D, Miotello A. Mesoporous Co-B nanocatalyst for efficient hydrogen production by hydrolysis of sodium borohydride. International Journal of Hydrogen Energy. 2013;38:14685-92.
[68] Ma H, Ji W, Zhao J, Liang J, Chen J. Preparation, characterization and catalytic $NaBH_4$ hydrolysis of Co-B hollow spheres. Journal of Alloys Componds 2009;474:584-

9.
[69] Tong D, Han X, Chu W, Chen H, Ji X. Preparation and characterization of Co-B flowers with mesoporous structure. Materials Research Bulletin. 2008;43:1327-36.
[70] Wu Z, Ge S. Facile synthesis of a Co-B nanoparticle catalyst for efficient hydrogen generation via borohydride hydrolysis. Catalysis Communications. 2011;13:40-3.
[71] Patel N, Fernandes R, Guella G, Kale A, Miotello A, Patton B, et al. Structured and nanoparticle assembled Co-B thin films prepared by pulsed laser deposition: a very efficient catalyst for hydrogen production. The Journal of Physical Chemistry C. 2008;112:6968-76.
[72] Patel N, Fernandes R, Miotello A. Promoting effect of transition metal-doped Co-B alloy catalysts for hydrogen production by hydrolysis of alkaline $NaBH_4$ solution. Journal of Catalysis. 2010;271:315-24.
[73] Tian H, Guo Q, Xu D. Hydrogen generation from catalytic hydrolysis of alkaline sodium borohydride solution using attapulgite clay-supported Co-B catalyst. Jounal of Power Sources. 2010;195:2136-42.
[74] Guo Y, Dong Z, Cui Z, Zhang X, Ma J. Promoting effect of W doped in electrodeposited Co-P catalysts for hydrogen generation from alkaline $NaBH_4$ solution. International Journal of Hydrogen Energy. 2012;37:1577-83.
[75] Krishnan P, Advani S, Prasad A. Thin-film CoB catalyst templates for the hydrolysis of $NaBH_4$ solution for hydrogen generation. Applied Catalysis B: Environmental. 2009;86:137-44.
[76]Nie M, Zou Y, Huang Y, Wang J. Ni-Fe-B catalysts for $NaBH_4$ hydrolysis. International Journal of Hydrogen Energy. 2012;37:1568-76.
[77] Kojima Y, Suzuki K, Kawai Y, Hydrogen generation from lithium borohydride solution over nano-sized platium dispersed on $LiCoO_2$. Journal of Power Sources. 2006;155:325-8.
[78] Zhang J, Delgass W, Fisher T, Gore J. Kinetics of Ru-catalyzed sodium borohydride hydrolysis. Journal of Power Sources. 2007;164:772-81.
[79] Özkar S, Zahmakiran M, Hydrogen generation from hydrolysis of sodium borohydride using Ru(0) nanoclusters as catalyst. Journal of Alloys Componds. 2005;404–406:728-31.
[80] Pena-Alonso R, Sicurelli A, Callone E, Carturan G, Raj R. A picoscale catalyst for hydrogen generation from $NaBH_4$ for fuel cells. Journal of Power Sources. 2007;165:315-23.
[81] Xu D, Dai P, Liu X, Cao C, Guo Q. Carbon-supported cobalt catalyst for hydrogen generation from alkaline sodium borohydride solution. Journal of Power Sources. 2008;182:616-20.

[82] Loghmani M, Shojaei A. Hydrogen generation from hydrolysis of sodium borohydride by cubic Co-La-Zr-B nano particles as novel catalyst. International Journal of Hydrogen Energy. 2013;38:10470-8.
[83] Zhang Q, Wu Y, Sun X, Ortega J, Kinetics of Catalytic Hydrolysis of Stabilized Sodium Borohydride Solutions. Industrial Engineering Chemistry Research. 2007;46: 1120-4.